IOP Conf. Series: Materials Science and Engineering **252** (2017) 012074 doi:10.1088/1757-899X/252/1/012074

# ELEMENTS OF CAM'S SYNTHESIS FOR A DISTRIBUTION MECHANISM FOR THE MILLER-ATKINSON CYCLE

**[1]Dragomir Ionuț, [1]Mănescu, Bogdan, [2]Stănescu, Nicolae–Doru, [2]Pandrea, Nicolae, [2]Clenci, Adrian, [2]Popa, Dinel**

[1]AKKA ROMSERV Bucharest, Romania, [2]University of Pitești, Pitești, Romania

s_doru@yahoo.com

**Abstract**. In this paper we present the synthesis of the cam for a distribution mechanism used for Miller-Atkinson cycle and described in previous works. The input data contain the angles at which the valve opens and closes, respectively, the dimensions of the main parts, the maximum displacement of the valve. and the law of motion of the valve. The authors consider that the law of motion of the valve is described by numerical values, even if in the simulation process they use analytical formulae for this displacement. The head of the valve is considered to be circular. A particular case of flat head of the valve is also described. The relative displacement of the lever and the valve is discussed in two hypotheses: symmetric position and asymmetric position of the contact point with respect to the axis of the valve. The contact between the head of the valve is assured by a cylindrical roller. The contact between the cam and the lever is considered with a roller tappet. In all cases the cam is obtained by numerical synthesis using a convenient angular degree. A great attention is paid to the convexity of the cam. The resulted cam is transformed in a convex one using the Jarvis March. The authors also perform a comparison between the theoretical profile of the cam and the profile of the convex cam. The reduced velocity and acceleration are obtained in all cases. Some aspects of the wear are discussed using the relative linear and angular velocities. The paper closes with a paragraph of conclusions.

## 1. Introduction

Some advantages of the Miller-Atkinson [1-8] cycle are given in [9, 10] and we will not repeat the presentation here.

Some experiments using intake valve closure are described in [11] leading to the increase of indicated thermal efficiency. For a diesel engine [12] the authors study the influence of Miller cycle and variable geometry turbocharger on combustion and emissions in steady and transient operation. An excellent review exploring the critical problems, challenges and prospective for the Miller-Atkinson cycle is given in [13]. Comparison between the Miller cycle and five stroke cycle is analyzed in [14] highlighting the advantage of the first at low loads in terms of fuel conversion efficiency. The application of the Miller cycle in the case of a hydrogen engine is presented in [15]. Gonca [16] performs a comparison between different types of engines from the point of view of the thermal efficiency, dimensionless power output and dimensionless power density. The authors [17] investigate the effects of compression ratio, intake valve closing retardation angle, and engine speed on the fuel

Content from this work may be used under the terms of the Creative Commons Attribution 3.0 licence. Any further distribution of this work must maintain attribution to the author(s) and the title of the work, journal citation and DOI.
Published under licence by IOP Publishing Ltd

consumption performance and power performance of the Miller cycle engine. Thermodynamic analysis of Otto engines working after Miller cycle is performed in [18], while the influence of engine design and operating parameters for a diesel engine working after the same cycle is analyzed in [19].

## 2. The mechanism

The mechanism in the asymmetric displacement of the lever (asymmetric case) is drawn in Fig. 1 and consists in the bar $OB$ of length equal to $l_1$ and having at its end a roll of radius $R_2$. In the initial position, the angle between the bar and the horizontal direction is $\beta_0$ and it is considered as known. The roll of radius $R_2$ is in contact, at any moment, with the head of the valve, head considered as an arc of radius $R_1$. The center of the arc is always situated at the distance $d$, considered known, from the vertical axis.

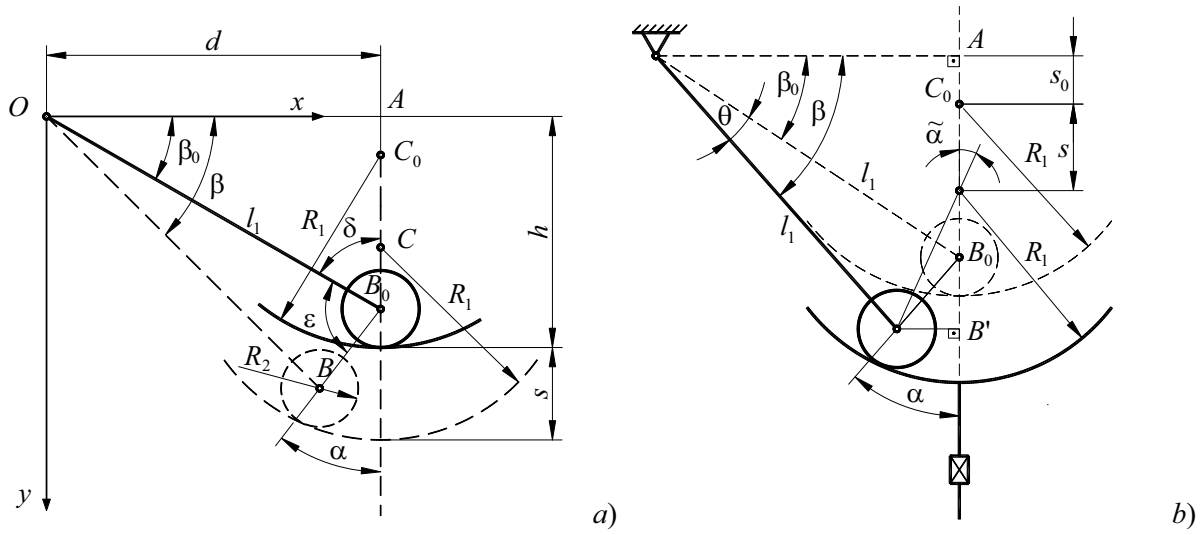


**Figure 1.** The mechanism in the asymmetric case: *a*) analytic approach; *b*) geometric approach.

The valve moves in the vertical direction with the displacement $s$ leading to the motion of the point $C$ (the center of the arc) from the point $C_0$ (the initial position) to the point $C$ (the current position). The distance between the point $C$ and the vertical axis $Oy$ remains equal to $d$.

The bar (lever) $OB$ of length $l_1$ rotates around the point $O$ such that the roll of radius $R_2$ remains all the time tangent to the arc of radius $R_1$. The new angle between the lever and the horizontal direction is $\beta$.

In an analytical approach the equation which offers the angle $\beta$ reads [9]

$$\begin{aligned}&\left\{2x_C\left(l_1\sin\beta - y_C\right)^2 + \left(l_1\cos\beta - x_C\right)\left[C_1 - 2y_C\left(l_1\sin\beta - y_C\right)\right]\right\}\\ &\quad - \left(l_1^2 + x_C^2 + y_C^2 - 2l_1x_C\cos\beta - 2l_1y_C\sin\beta\right)\\ &\times\left\{4x_C^2\left(l_1\sin\beta - y_C\right)^2 + \left[C_1 - 2y_C\left(l_1\sin\beta - y_C\right)\right]^2 - 4R_1^2\left(l_1\sin\beta - y_C\right)\right\} = 0,\end{aligned} \tag{1}$$

where

$$C_1 = R_1^2 - R_2^2 + l_1^2 - \left(x_C^2 + y_C^2\right), \tag{2}$$

$$x_C = d,\ y_C = h + s - R_1. \tag{3}$$

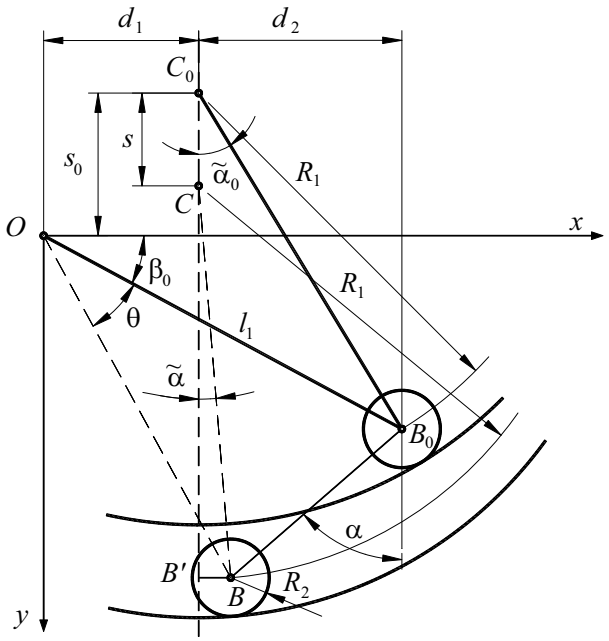


**Figure 2.** The mechanism in the symmetric case.

The geometric approach of the same case [10] offers the equation

$$-s + l_1\left[\sin(\theta + \beta_0) - \sin\beta_0\right] + (R_1 - R_2)(1 - \cos\tilde{\alpha}) = 0\,, \tag{4}$$

where

$$\tilde{\alpha} = \arcsin\left(\frac{l_1\left[\cos\beta_0 - \cos(\beta_0 + \theta)\right]}{R_1 - R_2}\right). \tag{5}$$

For the symmetric case (Fig. 2) we may write the following relations

$$\beta_0 = \arccos\left(\frac{d_1 + d_2}{R_1}\right), \tag{6}$$

$$\tilde{\alpha}_0 = \arcsin\left(\frac{d_2}{R_1}\right), \tag{7}$$

$$\alpha = \beta_0 + \frac{\theta}{2}\,, \tag{8}$$

$$B_0B = \tilde{d} = 2R_1\sin\left(\frac{\theta}{2}\right), \tag{9}$$

$$\sin\tilde{\alpha} = \frac{d_2 - \tilde{d}\sin\alpha}{R_1}\,, \tag{10}$$

$$\widetilde{\alpha} = \arcsin\left(\frac{d_2 - 2R\sin\alpha\sin\left(\frac{\theta}{2}\right)}{R_1}\right), \tag{11}$$

$$CB' = R_1\cos\widetilde{\alpha}, \tag{12}$$

$$C_0B' = R_1\cos\widetilde{\alpha}_0 + \widetilde{d}\cos\alpha, \tag{13}$$

$$s = C_0B' - CB', \tag{14}$$

$$s = R_1\cos\widetilde{\alpha}_0 - R_1\cos\widetilde{\alpha} + 2R_1\cos\alpha\sin\left(\frac{\theta}{2}\right). \tag{15}$$

The symmetry implies

$$\widetilde{\alpha}_{final} = \widetilde{\alpha}_f = -\alpha_0, \tag{16}$$

wherefrom

$$\sin\widetilde{\alpha}_f = \frac{d_2 - 2R_1\sin\alpha\sin\left(\frac{\theta}{2}\right)}{R_1} = -\sin\alpha_0, \tag{17}$$

$$d_2 - 2R_1\sin\left(\beta_0 + \frac{\theta}{2}\right)\sin\left(\frac{\theta}{2}\right) = -d_2, \tag{18}$$

$$2d_2 = R_1\left[\cos\beta_0 - \cos(\beta_0 + \theta)\right], \tag{19}$$

$$\theta_f = \arccos\left(\frac{R_1\cos\beta_0 - 2d_2}{R_1}\right) - \beta_0, \tag{20}$$

$$\theta_f = \arccos\left(\frac{d_1 - d_2}{R_1}\right) - \beta_0. \tag{21}$$

The calculation would be complete if we would know the distance $d_2$.

Assuming that the maximum displacement of the valve $s_{\max}$ is known, for the calculation of the distance $d_2$ we proceed as follows:

1. we consider $d_2 = kd_1$, with $k = 0.002$;
2. we calculate in order:

– $\beta_0$ with relation (6),
– $\widetilde{\alpha}_0$ with relation (7),
– $\theta_f$ with relation (21),
– $\alpha$ with relation (8),
– $s$ with relation (15),
– the deviation $\Delta$ with the formula

$$\Delta = s - s_{\max}; \tag{22}$$

3. if $|\Delta| > \varepsilon$, where $\varepsilon$ is the a priori imposed error, we consider a new value for $d_2$,

$$d_2 \mapsto d_2 + kd_1 \tag{23}$$

and repeat the step 2; otherwise the distance $d_2$ was determined.

## 3. Synthesis of the cam

For the repose position (Fig. 3, *a*)) we have

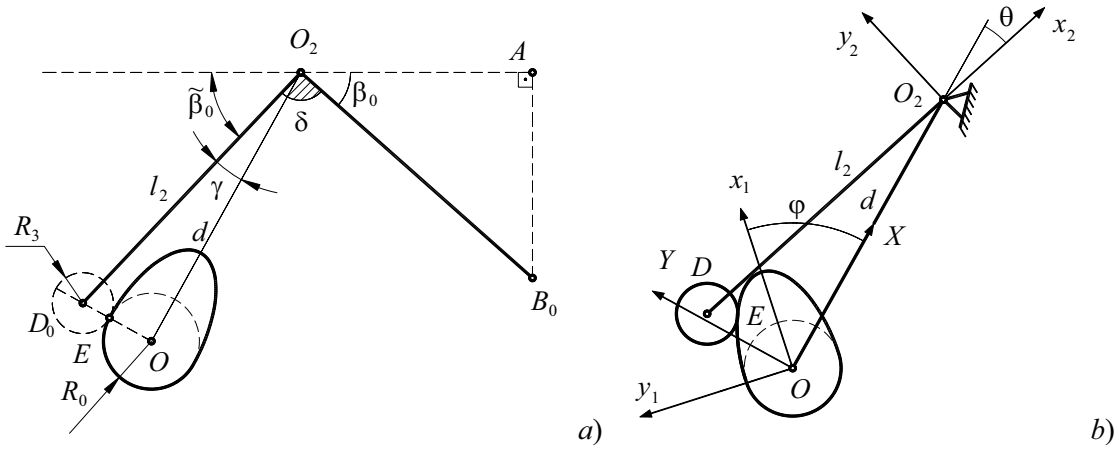


**Figure 3.** Synthesis of cam: *a*) repose position; *b*) current position

$$\widetilde{\beta}_0 = \pi - \beta_0 - \delta_0, \tag{24}$$

$$\gamma = \arccos\left(\frac{l_2^2 + d^2 - (R_0 + R_3)^2}{2l_2 d}\right). \tag{25}$$

Following the steps described in [10], the parametric equations of the cam (Fig. 3, *b*)) are

$$x_1 = d\cos\varphi - l_2\cos(\theta + \gamma + \varphi) - R_3\sin(\theta + \gamma + \varphi + \lambda), \tag{26}$$

$$y_1 = -d\sin\varphi + l_2\sin(\theta + \gamma + \varphi) - R_3\cos(\theta + \gamma + \varphi + \lambda), \tag{27}$$

where the parameter $\lambda$ is given by

$$\tan\lambda = \frac{d\cos(\theta + \gamma) - l_2\left(1 + \dfrac{\mathrm{d}\theta}{\mathrm{d}\varphi}\right)}{d\sin(\theta + \gamma)}. \tag{28}$$

## 4. Numerical analysis

We consider the case defined by $l_1 = 0.01612\,\mathrm{m}$, $R_1 = 0.025\,\mathrm{m}$, $R_2 = 0.010\,\mathrm{m}$, $\beta_0 = 15^0$, $s_{\max} = 0.00935\,\mathrm{m}$, $R_0 = 0.018\,\mathrm{m}$, $d = 0.042\,\mathrm{m}$, $l_2 = 0.060\,\mathrm{m}$, $R_3 = 0.01867\,\mathrm{m}$, $d_1 = 0.010\,\mathrm{m}$, the

angles $\varphi_1 = 92^0$ (when the valve starts to open), $\varphi_2 = 161^0$ (when the valve is completely open), $\varphi_3 = 180^0$ (when the valve starts to close), and $\varphi_4 = 244^0$ (when the valve is completely closed).

Two laws of motion are considered for the valve displacement

$$s_1(\varphi) = \begin{cases} 0 \text{ for } \varphi \in [0, \varphi_1), \\ s_{\max} \sin^2\left(\dfrac{90(\varphi - \varphi_1)}{\varphi_2 - \varphi_1}\right) \text{for } \varphi \in [\varphi_1, \varphi_2], \\ s_{\max} \text{ for } \varphi \in (\varphi_2, \varphi_3), \\ s_{\max} \sin^2\left(\dfrac{90(\varphi + \varphi_4 - 2\varphi_3)}{\varphi_4 - \varphi_3}\right) \text{for } \varphi \in [\varphi_3, \varphi_4], \\ 0 \text{ for } \varphi \in (\varphi_4, 360] \end{cases} \tag{29}$$

and

$$s_1(\varphi) = \begin{cases} 0 \text{ for } \varphi \in [0, \varphi_1), \\ s_{\max} \dfrac{(\varphi - \varphi_1)^2(\varphi - 2\varphi_2 + \varphi_1)^2}{(\varphi_2 - \varphi_1)^4} \text{ for } \varphi \in [\varphi_1, \varphi_2], \\ s_{\max} \text{ for } \varphi \in (\varphi_2, \varphi_3), \\ s_{\max} \dfrac{(\varphi - \varphi_4)^2(\varphi - 2\varphi_3 + \varphi_4)^2}{(\varphi_3 - \varphi_4)^4} \text{ for } \varphi \in [\varphi_3, \varphi_4], \\ 0 \text{ for } \varphi \in (\varphi_4, 360]. \end{cases} \tag{30}$$

The angle of rotation for the lever is determined from equation (1) in the asymmetric case.

For the symmetric case, the angle $\theta$ is obtained from the relation (15)

$$\sin\left(\frac{\theta}{2}\right) = \frac{s - R_1 \cos\tilde{\alpha}_0 - R_1 \cos\tilde{\alpha}}{2R_1 \cos\alpha}. \tag{31}$$

The resulted cams are presented in Figs. 4 and 5. The convex cams are obtained after the application of the Jarvis March. The original cams are drawn in blue, and the convex ones in red.

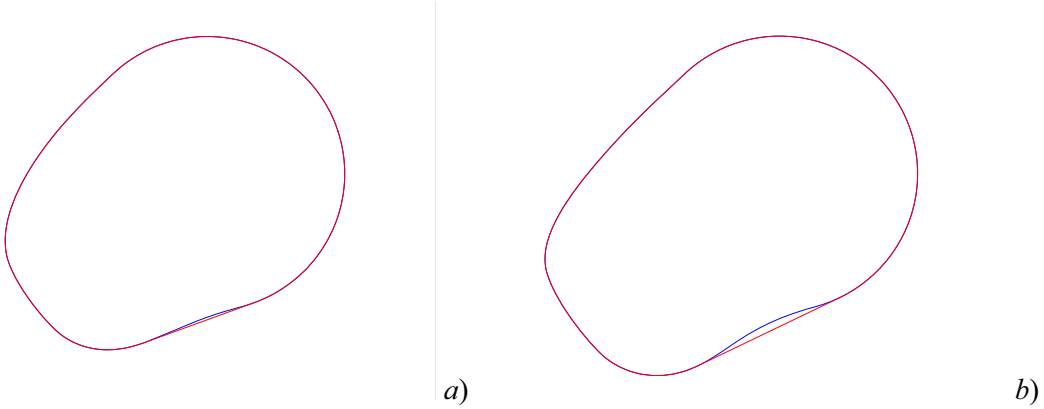

*a)* *b)*

**Figure 4.** The cam for the first law of motion: a) the asymmetric case; b) the symmetric case.

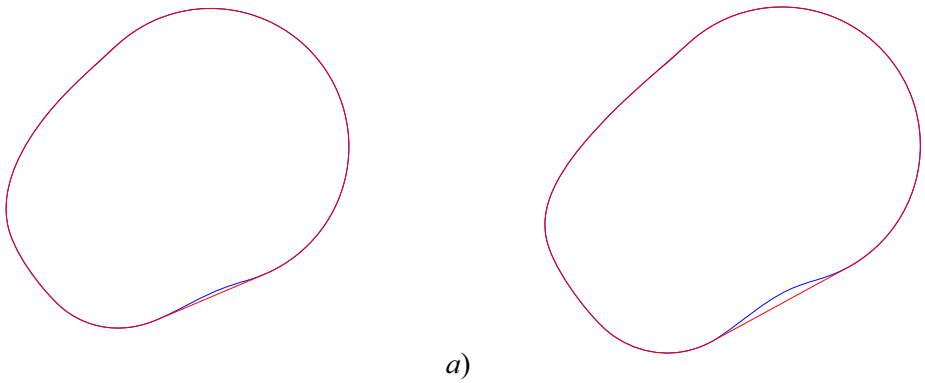

*a*) *b*)

**Figure 5.** The cam for the second law of motion: a) the asymmetric case; b) the symmetric case.

It is easy to observe that the symmetric case leads to a cam with bigger dimension no matter which law of motion is considered. Moreover, the obtained cam is not a convex one in all situation. The symmetric case leads to a more concave cam and the Jarvis March is constrained to avoid more characteristic points of the cam.

The reduced angular velocity and acceleration are given by

$$\left.\frac{\mathrm{d}\theta}{\mathrm{d}\varphi}\right|_{\varphi=\varphi_i} = \frac{\theta_{i+1} - \theta_{i-1}}{2\Delta\varphi}, \tag{32}$$

$$\left.\frac{\mathrm{d}^2\theta}{\mathrm{d}\varphi^2}\right|_{\varphi=\varphi_i} = \frac{\theta_{i+1} - 2\theta_i + \theta_{i-1}}{(\Delta\varphi)^2}. \tag{33}$$

The angular step $\Delta\varphi = 1^0 = \frac{\pi}{180}$ rad . The reduced angular velocity is a measure of the wear.

The diagrams are presented in Figs. 6–9.

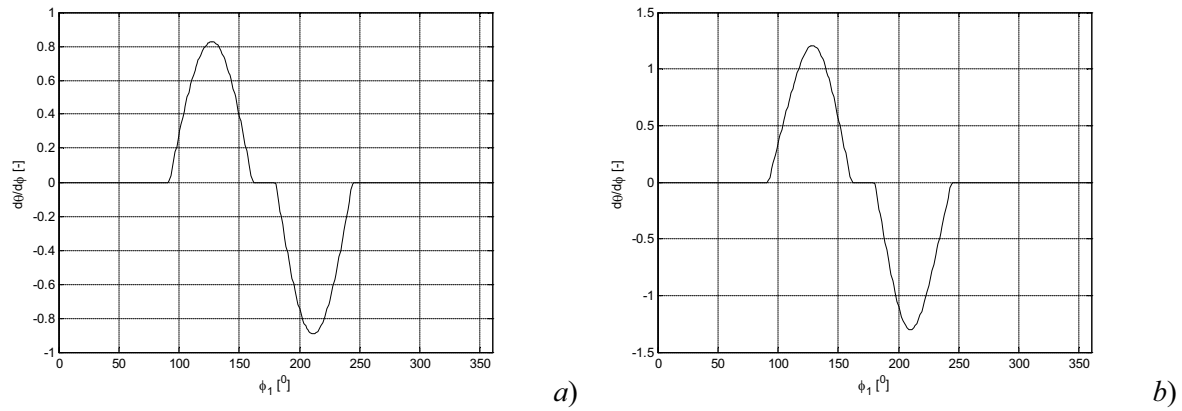


*a*) *b*)

**Figure 6.** The reduced angular velocity $\frac{\mathrm{d}\theta}{\mathrm{d}\varphi} = \frac{\mathrm{d}\theta}{\mathrm{d}\varphi}(\varphi)$ using the first law of motion for: *a*) the asymmetric case; *b*) the symmetric case.

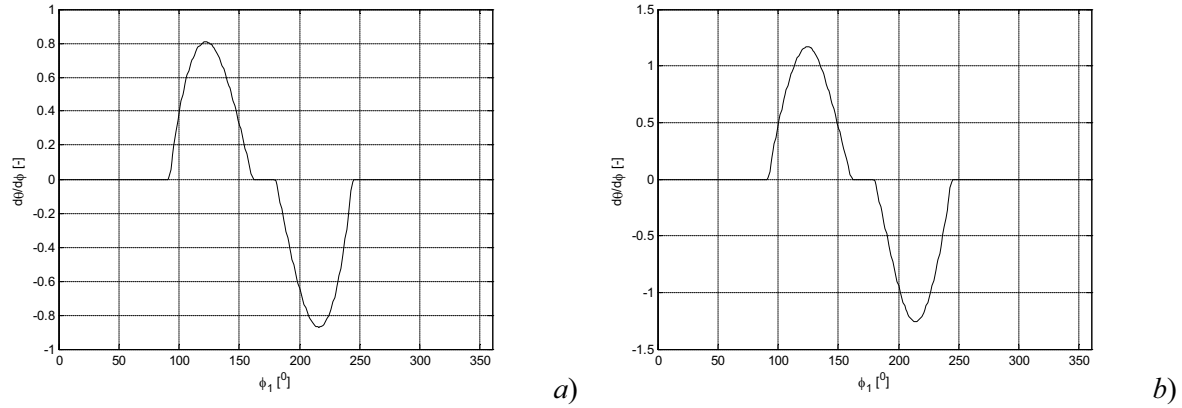


*a*) *b*)

**Figure 7.** The reduced angular velocity $\frac{\mathrm{d}\theta}{\mathrm{d}\varphi} = \frac{\mathrm{d}\theta}{\mathrm{d}\varphi}(\varphi)$ using the second law of motion for: *a*) the asymmetric case; *b*) the symmetric case.

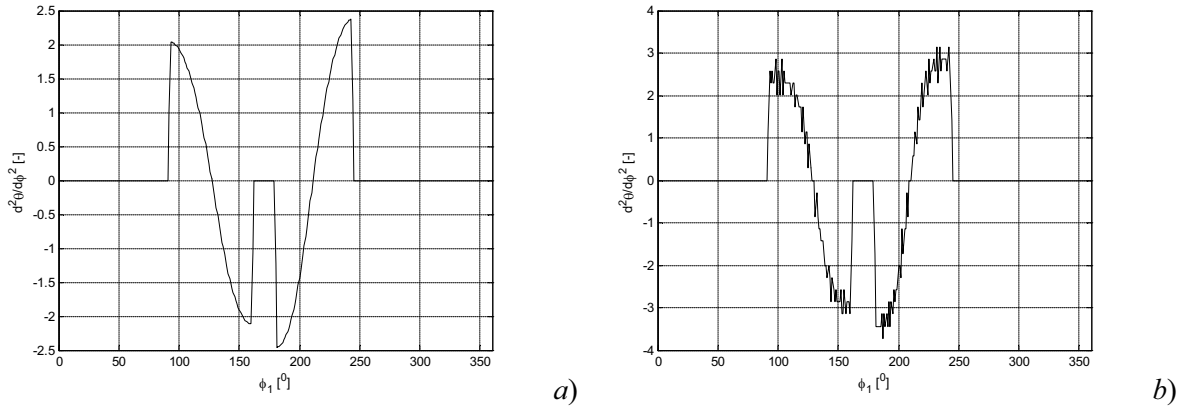


*a*) *b*)

**Figure 8.** The reduced angular acceleration $\frac{\mathrm{d}^2\theta}{\mathrm{d}\varphi^2} = \frac{\mathrm{d}^2\theta}{\mathrm{d}\varphi^2}(\varphi)$ using the first law of motion for: *a*) the asymmetric case; *b*) the symmetric case.

## 5. Planar head of valve

For the case of the planar head of valve (Fig. 10), some simple geometric considerations lead to the following expression for the angle $\theta$

$$\theta = \beta - \beta_0 = \arcsin\left(\frac{s + l_1 \sin\beta_0}{l_1}\right) - \beta_0 \tag{34}$$

The reduced angular velocity and acceleration may be obtained by direct calculation

$$\frac{\mathrm{d}\theta}{\mathrm{d}\varphi} = \frac{\mathrm{d}\theta}{\mathrm{d}s}\frac{\mathrm{d}s}{\mathrm{d}\varphi} = \frac{1}{\sqrt{1 - \left(\frac{s + l_1 \sin\beta_0}{l_1}\right)^2}}\frac{\mathrm{d}s}{\mathrm{d}\varphi}. \tag{35}$$

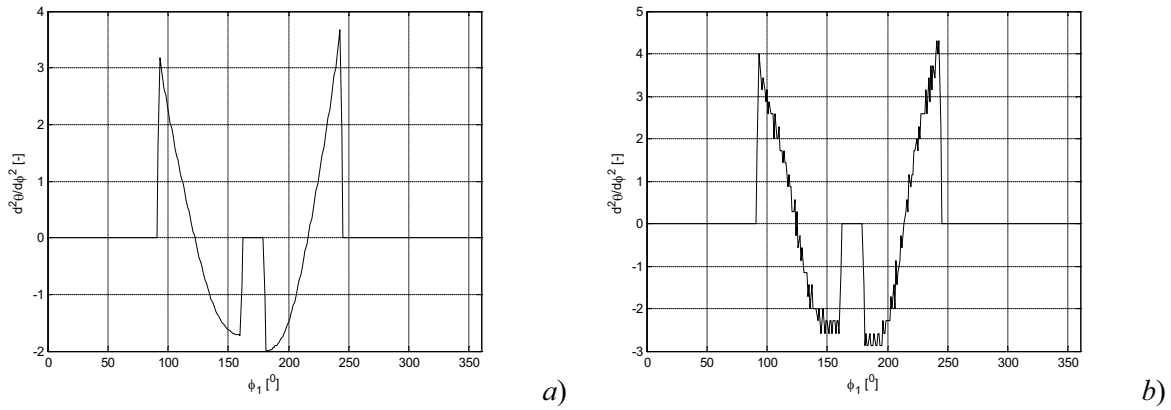


**Figure 9.** The reduced angular acceleration $\frac{d^2\theta}{d\varphi^2} = \frac{d^2\theta}{d\varphi^2}(\varphi)$ using the second law of motion for: *a*) the asymmetric case; *b*) the symmetric case.

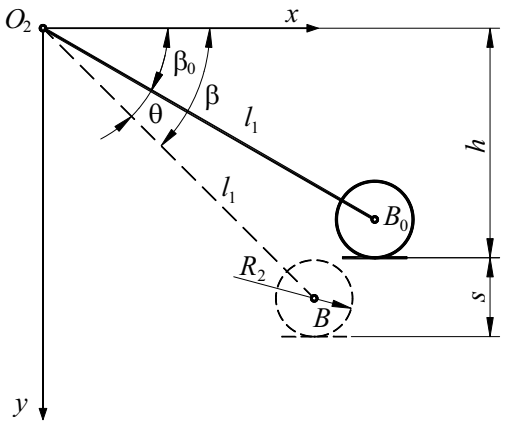


**Figure 10.** The case of the flat head of valve.

The cams obtained for the two laws of motion are captured in Fig. 11.

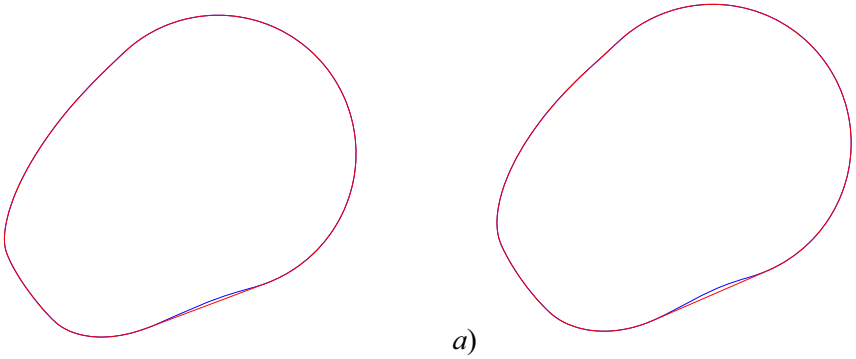


**Figure 11.** The cam for the flat head of valve: a) the first law of motion; b) the second law of motion.

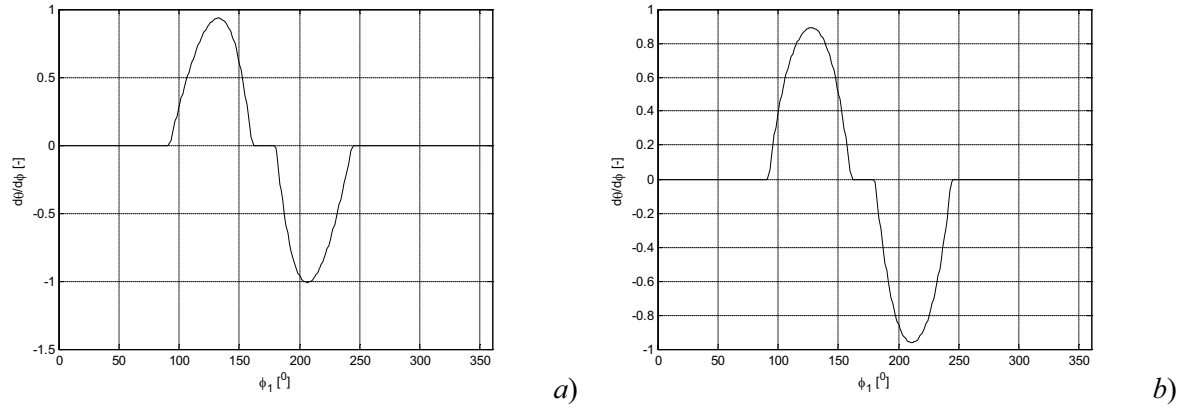


*a*) *b*)

**Figure 12.** The reduced angular velocity $\frac{d\theta}{d\varphi} = \frac{d\theta}{d\varphi}(\varphi)$ using: *a*) the first law of motion; *b*) the second law of motion.

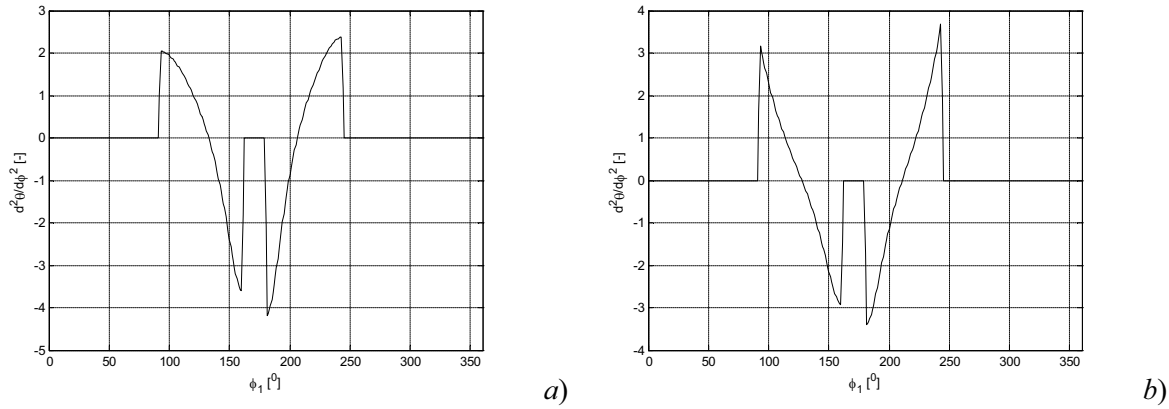


*a*) *b*)

**Figure 13.** The reduced angular acceleration $\frac{d^2\theta}{d\varphi^2} = \frac{d^2\theta}{d\varphi^2}(\varphi)$ using: *a*) the first law of motion; *b*) the second law of motion.

The corresponding diagrams are given in Fig. 12–13. The reader may observe the increase of the smoothness of the variation diagrams for the reduced angular velocity and acceleration.

## 6. Conclusions

From the previous diagrams we may conclude that, in the numerical case considered in this paper, the asymmetric case leads to a more smooth variation of the reduced angular velocity and acceleration and to cams with smaller dimensions than those obtained in the symmetric case. The symmetric case offers smaller bending moments acting on the valve comparing to the asymmetric case. The best situation is in the case of the flat head of valve.

Some future studies must be performed in order to obtain more smooth diagrams of variation for the reduced velocity and acceleration either by studying the influence of different parameters, or by considering more laws of motion for the valve. A great attention must be paid to the error in the law of motion caused by the Jarvis March which changes the profile of the cam. The best situation is that in which the obtained cam is a convex one. These aspects will be discussed in our next papers.

**References**

[1] Gonca G, Sahin B, Parlak A, Ust Y, Ayhan V, Cesur I and Boru, B, 2015, Theoretical and experimental investigation of the Miller cycle diesel engine in terms of performance and emission parameters, *Applied Energy* **138** 2015 11–20

[2] Martins MES and Lanzanova TDM, 2015, Full-load Miller cycle with ethanol and EGR: Potential benefits and challenges, *Applied Thermal Engineering* 274–85

[3] Ebrahimi R, 2011, Effects of mean piston speed, equivalence ratio and cylinder wall temperature on performance of an Atkinson engine, *Mathematical and Computer Modelling* **53** 1289–97

[4] Zammit JP, McGhee MJ, Shayler PJ, Lawa T and Pegg I, 2015, The effects of early inlet valve closing and cylinder disablement on fuel economy and emissions of a direct injection diesel engine, *Energy* **79** 100–10

[5] Murata Y, Kusaka J, Odaka M, Daisho Y, Kawano D, Suzuki H, Ishii H and Goto Y, 2006, Achievement of medium engine speed and load premixed diesel combustion with variable valve timing, *SAE paper 2006-01-0203*

[6] De Ojeda W, 2010, Effect of variable valve timing on diesel combustion characteristics, *SAE paper 2010-01-1124*

[7] Kéromnčs A, Delaporte B, Schmitz G and Le Moyne L, 2014, Development and validation of a 5 stroke engine for range extenders application, *Energy Conversion and Management* **82** 259–67.

[8] Zhu S, Deng K, Liu S and Qu S, 2015, Comparative analysis and evaluation of turbocharged Dual and Miller cycles under different operating conditions, *Energy* **93** 75–87

[9] Dragomir I, Mănescu B and Stănescu ND, 2017, The Analysis of a Distribution Mechanism for the Miller-Atkinson Cycle, *AVMS 2017*, Timișoara

[10] Dragomir I, Mănescu B, Stănescu ND and Pandrea N, 2017, Synthesis of the cam and determination of the reduced angular velocity and acceleration of the lever of a distribution mechanism for a Miller – Atkinson cycle, *ICMSAV XLI*, Cluj-Napoca

[11] Yan B, Wang H, Zheng Z, Qin Y and Yao M, 2017, The effects of LIVC Miller cycle on the combustion characteristics and thermal efficiency in a stoichiometric operation natural gas engine with EGR, *Applied Thermal Engineering* **122** 439–50

[12] Wu B, Zhan Q, Yu X, Lv G, Nie X and Liu S, 2017, Effects of Miller cycle and variable geometry turbocharger on combustion and emissions in steady and transient cold process, *Applied Thermal Engineering* **118** 621–9

[13] Zhao J, Research and application of over-expansion cycle (Atkinson and Miller) engines – A review, 2017, *Applied Energy* **185** 300–19

[14] Li T, Wang B and Zheng B, 2016, A comparison between Miller and five-stroke cycles for enabling deeply downsized, highly boosted, spark-ignition engines with ultra expansion, *Energy Conversion and Management* **123** 140–52

[15] Luo Q and Sun B, 2016, Effect of the Miller cycle on the performance of turbocharged hydrogen internal combustion engines, *Energy Conversion and Management* **123** 209–17

[16] Gonca G, 2016, Comparative performance analyses of irreversible OMCE (Otto Miller cycle engine)-DiMCE (Diesel Miller cycle engine)-DMCE (Dual Miller cycle engine), *Energy* **109** 152–9

[17] Wang Y, Zu B, Xu Y, Wang Z and Liu J, 2016, Performance analysis of a Miller cycle engine by an indirect analysis method with sparking and knock in consideration, *Energy Conversion and Management* **119** 316–26

[18] Dobrucali E, 2016, The effects of the engine design and running parameters on the performance of a Otto–Miller Cycle engine, *Energy*, **103** 119–26

[19] Gonca G and Sahin B, 2016, The influences of the engine design and operating parameters on the performance of a turbocharged and steam injected diesel engine running with the Miller cycle, *Applied Mathematical Modelling*, **40** 3764–82.